

A non-equilibrium model for rapid finite deformation of hydrated soft biological tissue in uniaxial confined compression

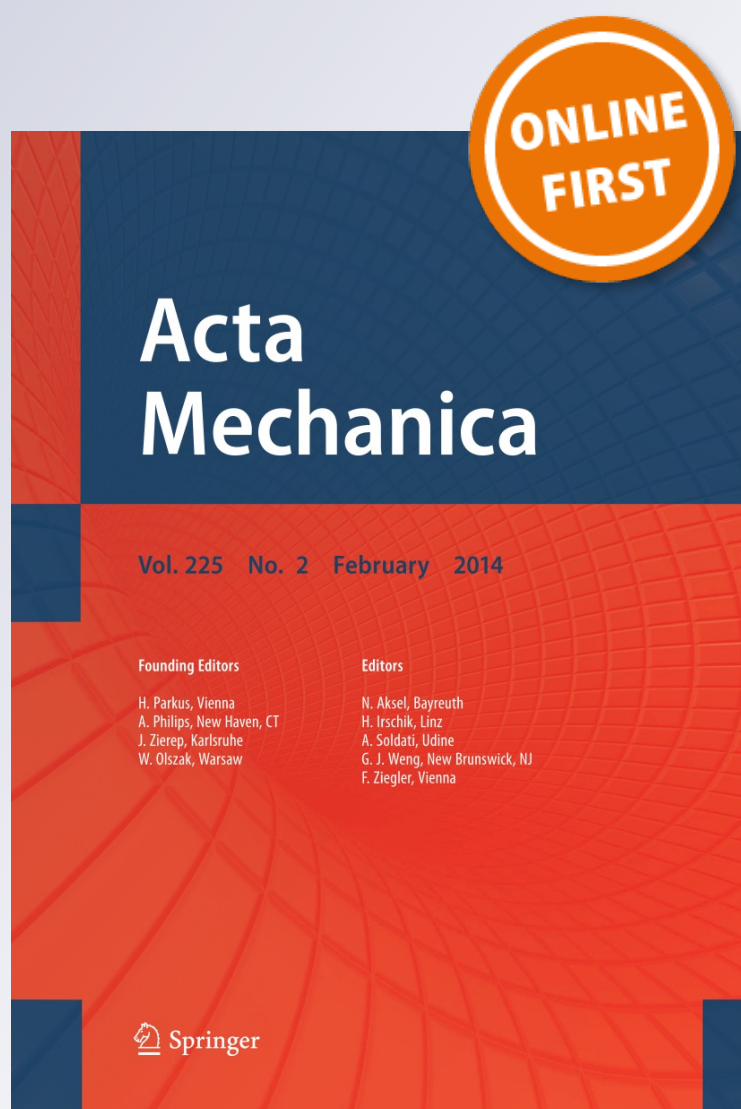
Henry W. Haslach

Acta Mechanica

ISSN 0001-5970

Acta Mech

DOI 10.1007/s00707-014-1100-x



Your article is protected by copyright and all rights are held exclusively by Springer-Verlag Wien. This e-offprint is for personal use only and shall not be self-archived in electronic repositories. If you wish to self-archive your article, please use the accepted manuscript version for posting on your own website. You may further deposit the accepted manuscript version in any repository, provided it is only made publicly available 12 months after official publication or later and provided acknowledgement is given to the original source of publication and a link is inserted to the published article on Springer's website. The link must be accompanied by the following text: "The final publication is available at link.springer.com".

Henry W. Haslach Jr.

A non-equilibrium model for rapid finite deformation of hydrated soft biological tissue in uniaxial confined compression

Received: 3 September 2013 / Revised: 20 January 2014
© Springer-Verlag Wien 2014

Abstract The viscoelastic behavior of hydrated soft biological tissue is strongly influenced by the mechanical interaction of its interstitial fluid with the solid phase. The classical uniaxial steady biphasic theory for soft tissue with high moisture content under confined compression is extended by replacing the Darcy steady flow assumption with an unsteady internal fluid flow model that involves an unsteady flow coefficient based on non-equilibrium thermodynamics. The finite deformation, non-equilibrium, unsteady biphasic viscoelastic analysis derived from conservation of linear momentum, which includes the mass terms neglected in some steady models, produces a nonlinear hyperbolic partial differential equation for the solid phase displacements, with a finite propagation velocity of the disturbance from the plunger in contrast to the instantaneous propagation of the classical parabolic steady description for cartilage. For confined compression of a small cylinder of hydrated soft biological tissue, the new hyperbolic equation is solved for the solid phase local displacements during both loading and relaxation as a function of time and position by a finite difference scheme of Shampine. A parametric study shows the influence of the unsteady coefficient on the predicted behavior, for both a linear elastic and a linear viscoelastic solid phase and for a constant permeability, by a comparison of the respective solid phase displacement distributions at the end of a constant rate plunger displacement at 0.001/s, 1/s and 1,000/s. Models assuming the Darcy relation predict physically realistic responses only for slow rates. The concavity of the stress–time curve for the solid phase at the plunger during a constant displacement of the plunger even at slow rates may be adjusted from softening to hardening by increasing the unsteady coefficient to increase the drag force exerted by the fluid on the solid phase. Because of unsteady fluid flow, overshoot of the solid phase displacement may occur initially during relaxation and also again near the end of the approach to equilibrium. A Zener standard linear viscoelastic solid phase slows the relaxation to equilibrium in comparison with a linear elastic solid phase.

1 Introduction

Solid–fluid interactions in hydrated biological soft tissue, including permeability, are often studied by the confined compression experiment, but the sequence of specimen non-equilibrium states during confined compression has not been explicitly accounted for in the classical biphasic mixture model for this test. The non-equilibrium behavior is needed to describe physiological events, involving moderate to high strain rate compression of high water content soft tissue to large deformation, that occur in many non-equilibrium biomechanical processes such as foot cartilage compression during contact with the ground during ambulation, transient compression due to deformation waves in the brain during an external physical insult, and support of a force on the spinal disk.

H. W. Haslach Jr. (✉)
Department of Mechanical Engineering, University of Maryland, College Park, MD 20742, USA
E-mail: haslach@umd.edu

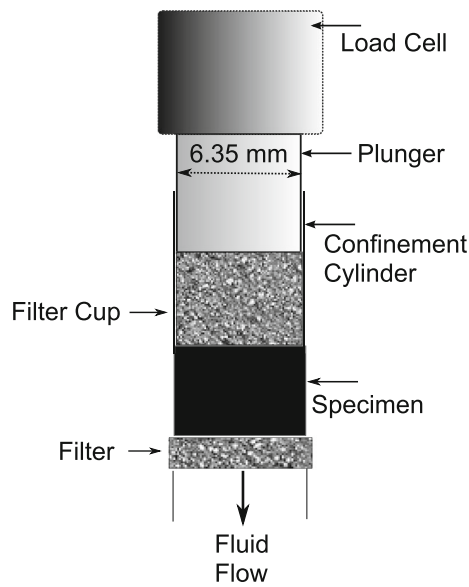


Fig. 1 Schematic of the fixture for a confined compression experiment. The reference coordinate, Z , is zero at the plunger and h at the base

A confined compression test may be idealized as a uniaxial loading of a specimen which is contained in a non-porous cylinder that prevents lateral deformation and ensures the nearly uniaxial flow of the internal fluid under the deformation. The plunger and/or the support at the opposite end are both porous to allow fluid transport from the specimen (Fig. 1). The typically assumed incompressibility of both the solid and the fluid components of the tissue implies that the observed uniaxial global deformation in a confined compression test is due to fluid loss so that the bulk tissue is compressible.

Biphasic, and the equivalent poroelastic, models capture aspects of the viscoelastic response of the bulk tissue introduced by the interaction of the solid and fluid phases. A biphasic or poroelastic mixture theory makes the approximation of Darcy steady internal fluid flow (e.g., [27]), which may be unrealistic when the hydrated soft tissue is subjected to moderate or high deformation rates. The standard biphasic model for confined compression (e.g., [10,21]) also neglects mass and acceleration terms, producing a governing parabolic nonlinear partial differential equation for the solid deformation, a modified diffusion equation, which predicts an unrealistic instantaneous response throughout the specimen when its surface is disturbed by the plunger. The parabolic nonlinear partial differential equation for the displacement determines the steady permeability of cartilage by least squares error curve fitting of the stress relaxation, measured by a load cell attached to the plunger, after a slow rate plunger displacement. Further, the equilibrium stress–strain relation is obtained from the final values of stress relaxation after different final displacements of the plunger (e.g., [1, Fig. 3]).

The small deformation, linear biphasic model of Mow et al. [21] extends by conservation of one-dimensional linear momentum to a large deformation, the nonlinear one by replacing the linearly elastic constitutive relation for the solid phase by a hyperelastic stress–stretch relation for an incompressible solid (e.g., [10,11]). The development is a mixture theory in which the fluid and solid are overlaid continua, but the phases are linked by the viscous drag on the solid due to the fluid motion. The large deformation model was validated by good fits to the response of bovine cartilage under very slow deformation up to 50% strain [1]. The steady model extends to tissue with a viscoelastic solid phase (e.g., [18]).

The classical steady models are shown, in Sect. 2, to produce physically unreasonable predictions for the response to moderate to high plunger displacement rates. Therefore, a novel, finite deformation, uniaxial unsteady biphasic model is derived in Sect. 3 that results in a nonlinear hyperbolic partial differential equation for the local solid phase displacements. This hyperbolic equation, which depends on the extension of the Darcy relation to non-equilibrium unsteady flow that involves an unsteady coefficient, predicts finite velocity of propagation through the tissue of the disturbance induced by the moving plunger at one end. The steady permeability continues to appear because steady flow is an attractor for the unsteady fluid flow as called for in the maximum dissipation non-equilibrium thermodynamics construction (Haslach [7,8]). The equation is solved numerically by a two-step Lax–Friedrichs finite difference scheme developed by Shampine [25], which

is outlined in Sect. 4. The final section explores consequences of the unsteady assumption on the predicted non-equilibrium response under various plunger displacement rates, permeability values, and constitutive relations for the solid phase. The behavior under a constant rate plunger displacement followed by stress relaxation while the plunger is held in place is described by the solid phase displacement distribution at the end of the plunger displacement regime, by the relation of time versus the stress in the solid phase at the plunger, and by the local displacements of the solid phase as the bulk tissue relaxes to equilibrium.

2 Steady biphasic model response to high strain rate

Models for confined compression that assume the Darcy relation are successful only for slow displacement rates of the plunger. At moderate and high displacement rates, the physically unreasonable response of classical steady biphasic models with parabolic governing equation, for a linearly elastic solid phase, verifies the necessity for a non-equilibrium unsteady biphasic model.

The mixture theory-based nonlinear parabolic differential equation for the reference state displacement, U , of the solid phase given by Holmes [10, Eq. 30] assumes Darcy steady interstitial fluid flow, large deformations of a specimen of length h , a hyperelastic solid material with stress–stretch relation, $\sigma_E(\lambda)$, for stretch λ , neglects the mass and body forces and assumes the mixture is homogeneous:

$$H(\lambda) \frac{\partial^2 U}{\partial Z^2} = \frac{\partial U}{\partial t} - v_o, \quad (1)$$

for the reference coordinate $0 \leq Z \leq h$, and $H(\lambda) = \frac{K}{\lambda} \left(\frac{\partial \sigma_E}{\partial \lambda} \right)$, for the intrinsic permeability K . The effect on the local solid phase displacement, $U(Z)$, of slow, moderate and high constant rate displacement, r , of the plunger follows by solving the Holmes equation numerically for a specimen of length, $h = 0.003$ m, using Mathematica NDSolve with initial conditions $U(0, Z) = (\partial U / \partial Z)(0, Z) = 0$ and boundary conditions $U(t, h) = 0$ and $U(t, 0) = rt$. The volume of fluid exiting per unit area is assumed to be $v_o = r$. At a slow rate deformation of 0.001/s up to 0.2 global strain, in other words, the plunger moves a distance equal to 20% of the specimen length, the Holmes equation for a linearly elastic solid having $E = 10$ or 550 kPa and permeability of 10^{-12} predicts in each case a local displacement field at the end of the ramp deformation that is the nearly uniform local stretch response corresponding to a quasi-static deformation, but with local stretches smaller than 0.8 both near the plunger and near the porous base and also a slightly larger stretch at the mid-region of the specimen.

The Holmes model at a moderate rate of 1/s up to strain 0.2, permeability of 10^{-16} and $E = 10$ kPa predicts a uniform displacement of 0.0006 throughout most of the specimen except near the fixed base so that the tissue segment near the plunger moves as a rigid unit with zero local strain, a stretch of 1, internal to the segment (Fig. 2a), which may be a consequence of the instantaneous transport associated with the parabolic model. Additionally, for the plunger to move through $0.2h$, fluid must leave the specimen, but the amount of fluid loss indicated by the non-uniform displacement near the base is not sufficient to account for that required by the plunger motion so that the prediction is physically unrealistic. The response is similar at 100/s for $E = 550$ kPa and permeability of 10^{-9} or 10^{-16} .

The Soltz and Ateshian [28] closed-form solution arises from the parabolic partial differential equation [21],

$$\frac{\partial^2 U}{\partial Z^2} = \frac{1}{H_A K} \frac{\partial U}{\partial t}, \quad (2)$$

for H_A the aggregate elastic modulus and K the permeability. Note that their equation does not have the v_o term of Holmes. The Soltz–Ateshian analysis assumes $Z = 0$ at the base and $Z = h$ at the plunger, while the converse is assumed in the derivation below of the unsteady biphasic model, so that here $h - Z$ is substituted for Z in their result to allow comparison. Their transformed initial condition is again $U(Z, 0) = 0$ and their transformed boundary conditions during the ramp are $U(h, t) = 0$ at the base and $U(0, t) = rt$ at the plunger, where r is the constant plunger displacement rate. Moderate- and high-rate displacements of the plunger, at 1/s or 1,000/s and $H_A K = 1.4 \times 10^{-8}$, introduce a wave in the solid phase displacements that implausibly oscillates from tension to compression at the end of the plunger displacement regime, probably due to the trigonometric functions of Z in their closed-form solution (Fig. 2b).

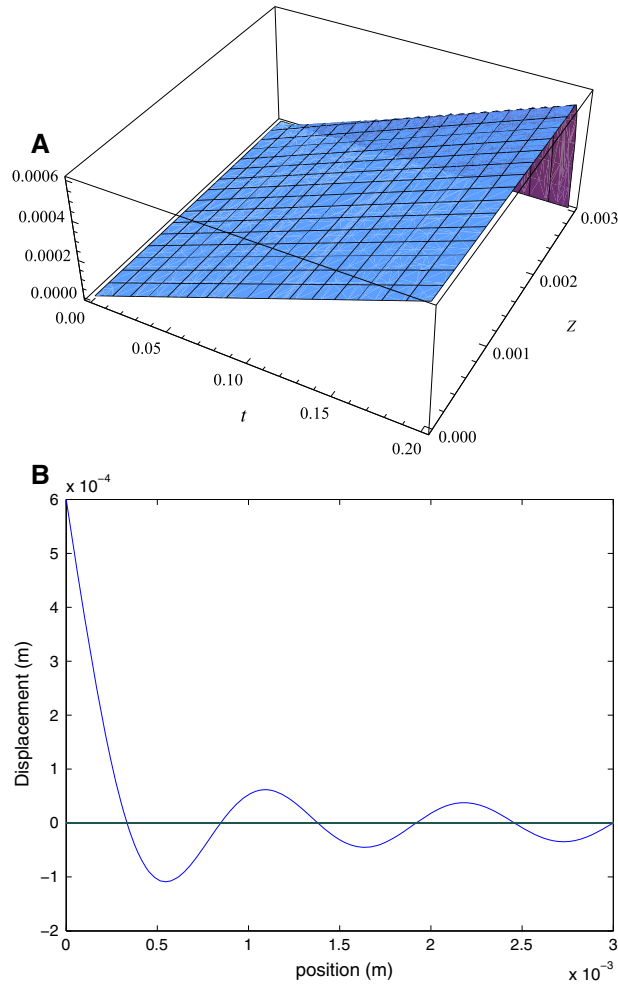


Fig. 2 a The local displacement, $U(t, Z)$, as a function of time and position on the specimen predicted by the Holmes model to a constant deformation at 1/s for $K = 10^{-12}$. The plunger is at $Z = 0$. **b** The predicted local solid phase displacements response of the Soltz–Ateshian model at the end of a constant plunger displacement to 0.2 global strain at 1,000/s for $K H_A = 1.4 \times 10^{-8}$. The plunger is at $Z = 0$

3 Viscoelastic, unsteady, biphasic model

The mixture theory development of the finite deformation, unsteady biphasic model from conservation of linear momentum is a modification of the nonlinear theory of Holmes [10], but allows a viscoelastic solid phase and does not neglect the masses of the fluid and solid phases. The unsteady flow of the fluid and the inclusion of the masses introduce a term involving the second partial derivative of the displacement with respect to time so that the resulting equation for the local displacements is no longer parabolic as is the Holmes equation.

The balance of linear momentum for either the solid or fluid phase, in the current (spatial) configuration, is

$$\rho D_t \mathbf{v} = \nabla \sigma + \boldsymbol{\pi} + \rho \mathbf{b}, \quad (3)$$

where ρ is the phase density, \mathbf{v} is the phase velocity, σ is the phase Cauchy stress, $\boldsymbol{\pi}$ is the diffusive drag per volume, and \mathbf{b} is the body force/mass. Recall that in the spatial configuration $D_t = \partial/\partial t + \mathbf{v} \cdot \nabla$. Neglecting the body force, (3) becomes for the solid and fluid phases, respectively,

$$\nabla \sigma^s + \boldsymbol{\pi}^s = \rho^s \dot{\mathbf{v}}^s \quad \text{and} \quad \nabla \sigma^f + \boldsymbol{\pi}^f = \rho^f \dot{\mathbf{v}}^f. \quad (4)$$

The inertia terms on the right are not neglected as they are in the steady theory that assumes that the mass is very small and acceleration is minimal. The fluid and solid drag forces are equal and opposite so that from mixture theory $\boldsymbol{\pi}^f = -\boldsymbol{\pi}^s$.

The solid and fluid phases are each assumed incompressible to write the respective masses in terms of the volume fractions. The continuity equation in the current configuration, where ϕ is the phase volume fraction, is then for either the solid or the fluid phase

$$\frac{\partial \phi}{\partial t} + \nabla \cdot (\phi \mathbf{v}) = 0. \quad (5)$$

All volume change is due to transport of fluid out of the specimen. Assume that the material is saturated so that $\phi^f + \phi^s = 1$. Adding the continuity equation (5) for the solid and for the fluid phases produces

$$\nabla \cdot (\phi^s \mathbf{v}^s + \phi^f \mathbf{v}^f) = 0. \quad (6)$$

3.1 Application to uniaxial loading

Assume uniaxial compressive loading. If the solid phase is elastic, the Cauchy stress for the solid, σ_E , is obtained from a hyperelastic strain energy density function that accounts for large deformations. If the solid is viscoelastic, the time-dependent stress is σ_v . The constitutive assumptions for the stress in the solid and in the fluid phases are, analogous to Eqs. (17) and (11b) found in Holmes [10],

$$\sigma^s = -\phi^s p + \sigma_v \quad \text{and} \quad \sigma^f = -\phi^f p, \quad (7)$$

where p is the hydrostatic pressure in the fluid. The pressure, p , arises from the requirement that the solid and the fluid are both incompressible. The total uniaxial stress, σ_t , at a point in the bulk specimen is the sum of the stresses in the fluid and in the solid,

$$\sigma_t = -p + \sigma_E; \quad \text{or} \quad \sigma_t = -p + \sigma_v. \quad (8)$$

Adding (4) for the fluid and the solid phases eliminates the drag force so that

$$\nabla \sigma^f + \nabla \sigma^s = \rho^s \dot{v}^s + \rho^f \dot{v}^f. \quad (9)$$

Substitution in (9) of the expressions for the respective Cauchy stresses from (7) and the fact that $\phi^s + \phi^f = 1$ imply,

$$\rho^s \dot{v}^s + \rho^f \dot{v}^f = \nabla(-p + \sigma_v) = \nabla \sigma_t. \quad (10)$$

This equation is essentially a statement of Newton's law per unit volume for the loaded specimen.

In the uniaxial case, for spatial uniaxial coordinate z , (10) becomes using (8),

$$-\frac{\partial p}{\partial z} + \frac{\partial \sigma_v}{\partial z} = \rho^s \dot{v}^s + \rho^f \dot{v}^f. \quad (11)$$

An expression for the stress in the solid phase requires a constitutive assumption for the diffusive drag force per volume acting on the solid,

$$\pi^s = p \nabla \phi^s - \pi_o. \quad (12)$$

Here the first term accounts for the gradient of the solid phase volume fraction and π_o accounts for the solid–fluid interaction that may involve normal and/or shear forces.

The linear theory of Mow et al. [21] assumes the simpler form $-\pi^s = \pi^f = k(v^s - v^f)$, where the diffusive drag coefficient, k , is constant. The diffusive drag coefficient, k , is related to the permeability coefficient, K , by $k = (\phi^f)^2/K$.

Here the further constitutive assumption is made that

$$\nabla p = (\phi^f)^{-2} \pi_o, \quad (13)$$

so that when combined with the Holmes [10] isotropic form $\pi_o = k(III_C)(v^s - v^f)$, where $C = F^t F$ and F is the deformation gradient of the solid phase, produces the Darcy law.

3.2 Unsteady uniaxial behavior

The general method employed here to account for unsteady fluid flow is to modify the steady Darcy relation. As a simple example of the technique, the Darcy relation is replaced by a linear ordinary differential equation (Haslach [7], [8, pp. 247–249]). In this construction, the steady Darcy relation defines the stationary manifold for generalized entropy production and the unsteady coefficient τ in (14) measures the speed of evolution of the fluxes to the relationship defined by the stationary manifold.

$$\tau \dot{Q} + Q = -K \nabla p, \quad (14)$$

for permeability coefficient K with units m^4/Ns , where τ has units of time, p is the local fluid pressure, and where $Q = v^f - v^s$ is the pointwise rate of volume flow per area of the fluid in m/s , i.e., the relative velocity. The unsteady coefficient $\tau = 0$ on the steady manifold, but otherwise the coefficient τ may depend on stretch or other variables. To make (14) objective in the spatial configuration, the unsteady relation is given in terms of the Lie time derivative,

$$\tau \mathcal{L}_{\mathbf{v}}(Q) + Q = -K \nabla p, \quad (15)$$

where \mathbf{v} is the velocity of the fluid. The Lie derivative, called the Lie time derivative, of a function f is the push forward of the directional derivative of the pullback of f to the reference configuration in the direction of the spatial velocity, \mathbf{v} , denoted $\mathcal{L}_{\mathbf{v}}(f) = \chi_*(D_{\mathbf{v}}\chi_*^{-1}(f))$ [12, p. 106], where $D_{\mathbf{v}}$ denotes the material time derivative and χ is the map from the reference to the spatial configuration. Therefore, the Lie time derivative pulls back to the material time derivative in the reference configuration.

Because of the assumption (13), the expression (15) becomes, in the spatial configuration,

$$\tau \mathcal{L}_{\mathbf{v}}(Q) + Q = -K(\phi^f)^{-2}\pi_o. \quad (16)$$

Rearrangement of (16) shows that the drag force in the spatial configuration is

$$\pi_o = -\frac{(\phi^f)^2}{K}[\tau \mathcal{L}_{\mathbf{v}}(Q) + Q]. \quad (17)$$

Clearly if $\tau = 0$ or if $\mathcal{L}_{\mathbf{v}}(Q) = 0$ so that the Darcy relation $Q = -K \nabla p$ holds, then the drag force $\pi_o = -(\phi^f)^2 K^{-1}(v^f - v^s)$.

3.3 Spatial configuration description

Using the constitutive relation (7), $\sigma^s = -\phi^s p + \sigma_v$, the product rule for $\partial(\phi^s p)/\partial z$, and (12), the linear momentum balance (4) for the solid phase, $\nabla \sigma^s + \pi^s = \rho^s \dot{v}^s$, becomes

$$-\phi^s \frac{\partial p}{\partial z} + \frac{\partial \sigma_v}{\partial z} - \pi_o = \rho^s \dot{v}^s, \quad (18)$$

To eliminate p from (18) apply (11), after writing $1 = \phi^f + \phi^s$ for the coefficient of $\partial \sigma_v / \partial z$:

$$\phi^f \frac{\partial \sigma_v}{\partial z} - \pi_o = \phi^f \rho^s \dot{v}^s - \phi^s \rho^f \dot{v}^f. \quad (19)$$

Therefore, momentum balance for the solid, from (19) and (17) is

$$\phi^f \frac{\partial \sigma_v}{\partial z} = \phi^f \rho^s \dot{v}^s - \phi^s \rho^f \dot{v}^f - K^{-1}(\phi^f)^2[\tau \mathcal{L}_{\mathbf{v}}(Q) + Q]. \quad (20)$$

The partial differential equation (20) is the main result of the spatial configuration analysis.

To introduce the local solid phase displacement into (20), first integrate the continuity Eq. (6) to $\phi^s v^s + \phi^f v^f = v_o$, where the velocity, $v_o(t)$, is a function of time only, and all the terms on the left side of the equation are functions of position and time. While v_o is obtained as an integration constant with respect to z , physically, v_o is the velocity in volume per cross-sectional area of the flow out of the sample. The model does

not distinguish whether fluid leaves the specimen at the plunger end or the base end. A simple computation shows that $v^s - v^f = (v^s - v_o)/\phi^f$. Also $v^s = \partial u(z, t)/\partial t$ in the spatial configuration. Therefore,

$$-Q = v^s - v^f = (v^s - v_o)/\phi^f = \frac{1}{\phi^f} \left(\frac{\partial u(z, t)}{\partial t} - v_o \right). \quad (21)$$

The construction generalizes the Holmes steady equation because if $\tau = 0$, then substituting $k = (\phi^f)^2/K$ in (20), letting σ_v be hyperelastic, σ_E , and neglecting the acceleration terms yields Eq. (18a) of Holmes [10],

$$\phi^f \frac{\partial \sigma_E}{\partial z} = k (v^s - v^f). \quad (22)$$

3.4 Reference configuration description

The constrained uniaxial deformation is $z = \chi(Z, t)$ defined by the relation $x = X$, $y = Y$, and $z = f(Z, t)$ between the reference coordinates (X, Y, Z) , where Z is the axial coordinate, and the spatial coordinates (x, y, z) . Let $U(Z, t)$ be the axial displacement in the reference coordinates, where $U(Z, t) = u(z(Z), t)$, and $z = Z + U(Z, t)$. The stretch is $\lambda = dz/dZ = 1 + \partial U/\partial Z$. Finally, Eq. (20) is written in terms of the displacement $U(Z, t)$.

By the chain rule,

$$\frac{\partial \sigma_v}{\partial z} = \frac{1}{\lambda} \frac{\partial \sigma_v}{\partial Z}.$$

In the hyperelastic case, if σ_E is obtained by differentiating an energy function with respect to stretch, it is the Piola stress, which can be easily be transformed to the second Piola stress. Apply the chain rule to the right-hand term

$$\frac{\partial \sigma_v}{\partial Z} = \frac{\partial \sigma_v}{\partial \lambda} \frac{\partial^2 U}{\partial Z^2}.$$

Because in the reference configuration, the Lie time derivative pulls back to the material time derivative, Eq. (20) in terms of $U(Z, t)$ becomes the nonlinear hyperbolic partial differential equation

$$\begin{aligned} & \frac{\Phi^f}{\lambda} \left(\frac{\partial \sigma_v}{\partial \lambda} \right) \frac{\partial^2 U}{\partial Z^2} - \left[\Phi^f \rho^s + \frac{(\Phi^s)^2}{\Phi^f} \rho^f + \tau K^{-1} (\Phi^f)^2 \right] \frac{\partial^2 U}{\partial t^2} \\ & + \left(\left[\Phi^s \rho^f + \tau K^{-1} (\Phi^f)^2 \right] \frac{\dot{\Phi}^f}{(\Phi^f)^2} - \frac{1}{\Phi^f} K^{-1} (\Phi^f)^2 \right) \frac{\partial U}{\partial t} \\ & = - \left[\Phi^s \rho^f + \tau K^{-1} (\Phi^f)^2 \right] \left[\frac{1}{\Phi^f} \frac{\partial v_o}{\partial t} - \frac{\dot{\Phi}^f}{(\Phi^f)^2} v_o \right] - \frac{k v_o}{\Phi^f}, \end{aligned} \quad (23)$$

where k is the drag coefficient, Φ^f and Φ^s are the volume fractions in the reference configuration, and τ is the unsteady coefficient.

Note that by (17), for example, the term $\tau K^{-1} (\Phi^f)^2$ has units of specific mass so that each term has units of force/volume. Because this product is a specific mass term, a smaller permeability or a larger τ increase the effective mass in the equation and thus the inertia. Zero τ would allow instantaneous fluid flow if the mass of the fluid and solid phases are also neglected since the inertia is then zero. Note that only the fluid mass appears in the coefficients of the linear and the constant terms. The applied time-dependent deformation rate occurs in the term on the right side of the equation through v_o .

A second equation is required because (23) is written in terms of the two unknown functions $U(Z, t)$ and $\Phi^s(Z, t)$. The volume change satisfies $J = \det(F) = \lambda(Z)$, for the deformation gradient, F , since the transverse stretches are equal to 1 in the idealized confined compression. By conservation of mass in the material configuration, for Φ_o^s the initial solid volume fraction, the solidity is

$$\Phi^s = \frac{\Phi_o^s}{J} = \frac{\Phi_o^s}{\lambda}. \quad (24)$$

This expression for the global average volume fraction can be computed directly under the assumption that the amount of fluid lost at time t is rtA and that the initial total volume is hA where r is the displacement rate of the plunger and h is the specimen length. If the volume fractions are global rather than local, the material is homogeneous. However, the pressure still may depend on position.

Therefore, the following terms in (23) depend on $\partial U/\partial Z$, denoted by U_Z to simplify notation:

$$\begin{aligned}\Phi^f &= 1 - \frac{\Phi_o^s}{1 + U_Z}; \\ \frac{\dot{\Phi}^f}{(\Phi^f)^2} &= \frac{\Phi_o^s U_{Zt}}{1 + U_Z - \Phi_o^s}; \\ \frac{(\Phi^s)^2}{\Phi^f} &= \frac{(\Phi_o^s)^2}{(1 + U_Z)(1 + U_Z - \Phi_o^s)}.\end{aligned}\quad (25)$$

The nonlinear hyperbolic partial differential equation (23) for $U(Z, t)$ is the main result of the analysis. The partial differential Eq. (23) would be quasi-linear hyperbolic if the volume fractions were constant in the coefficients because λ depends on $\partial U/\partial Z$. The nonlinearity is a consequence of the presence of the second-order partial $U_{Zt}(Z, t) = \partial^2 U/\partial Z \partial t$ in $\dot{\Phi}^f(Z, t)$. The unsteady biphasic model equation (23) predicts transport in finite time since it is hyperbolic.

The initial conditions are $U(Z, 0) = 0$, $U_Z(Z, 0) = 0$ and an assumption that $U_t(Z, 0) = -rZ/h + r$, where r is the constant rate of displacement of the plunger. The problem is solved subject to the boundary conditions $U(0, t) = d(t)$ and $U(h, t) = 0$, where $d(t)$ is the displacement of the face of the plunger as a function of time. For confined compression in the case of a linearly increasing plunger displacement at r , $d(t) = rt$, then $v_o = r$ and $\dot{v}_o = 0$.

Equation (23) also accounts for bulk stress relaxation by setting $r = 0$ so that the right side is zero and using as initial conditions the state at the end of the ramp load. The boundary conditions are that $U(0, t) = d(t_f)$ and $U(h, t) = 0$, where $d(t_f)$ is the final plunger displacement, and t_f is the time to perform the plunger displacement.

3.5 The meaning of τ

The maximum dissipation non-equilibrium thermodynamics construction of Haslach [8, p. 248] for the non-equilibrium flow of a fluid through a porous material guides the choice of the form of the expression

$$\tau \dot{Q} + Q = -K \nabla p, \quad (26)$$

where the positive coefficients τ , K do not depend explicitly on time, but ∇p may. Of course, non-equilibrium flow requires that $\nabla p \neq 0$, and these gradients may not be the same from point to point. The parameter τ controls the relaxation from unsteady to Darcy steady flow. In this non-equilibrium thermodynamic model, a fluid relaxes to steady state in a manner that produces maximum dissipation of a generalized entropy production function [8]. On the other hand, a solid relaxes to equilibrium in a manner that produces maximum dissipation of a generalized energy function. Interstitial fluid relaxation from unsteady to steady flow is a separate phenomenon from stress relaxation to equilibrium of a viscoelastic solid phase, but the two relaxations may influence each other.

The relaxation time within a chosen approximation of the steady flow state may be estimated from (26) after it is solved in closed form for ∇p is fixed, using an integrating factor and integration by parts, to obtain

$$Q(t) = Q(0) \exp(-t/\tau) - K \nabla p [1 - \exp(-t/\tau)] - \exp(-t/\tau) \int_0^t \exp(s/\tau) \frac{d(K \nabla p)}{ds} ds. \quad (27)$$

This expression predicts that the flow Q is smaller than it would be in steady flow for the same $K \nabla p$ with ∇p independent of time because the pressure must accelerate the fluid. For example, the time required to achieve 95% of the volume flux corresponding to steady flow is approximately, if the integral term is neglected (it is zero only in equilibrium) in (27), $\exp(-t/\tau) = 0.05$, or $t = -\tau \ln(0.05) = 2.996\tau$. Therefore, small τ quickly produces steady flow, which is consistent with the fact that in the defining flow equation $\tau = 0$ produces Darcy steady flow. This time is not the same as the relaxation time to within 5% of equilibrium.

For the numerical examples presented in Sect. 5, τ is assumed constant, but it is possible that τ could depend on other system parameters. In practical applications with the expression for τ depending on empirical parameters, curve fitting of the stress response at the plunger determines the value of τ just as it does in the classical use of the confined compression test to compute permeability.

Because fluid flow and interaction with the solid phase contribute to the viscoelastic response of hydrated soft biological tissue, the fluid flux within a high fluid content soft biological tissue under loads is sometimes identified as a viscoelastic process (e.g., Natali et al. [22]). Of course, this role of the fluid flux is well known experimentally from the original studies of the permeability of cartilage aided by the parabolic linear biphasic model [21]. Other forms for the unsteady relation (14) governing the fluid velocity might be chosen, but the one taken here is of the form assumed for the evolution of a viscous variable, q_i , given in some traditional viscoelastic models (e.g., [2,26]) as $\tau \dot{q}_i + q_i = \gamma \sigma_o$, where τ in units of time and γ in the necessary units are viscous parameters and σ_o is the stress response at a very high strain rate so that it approximates the instantaneous response.

4 Numerical technique

The finite differences numerical solution of the second-order hyperbolic partial differential equation (23) for $U(Z, t)$ is facilitated by transforming (23) to the system of first-order partial differential equations, $u_1 = U$, $u_2 = U_Z$ and $u_3 = U_t$, where $U_Z = \partial U / \partial Z$ and $U_t = \partial U / \partial t = g(Z, t, U, U_Z)$. The system of first-order partial differential equations is then $\dot{u}_1 = u_3$; $\dot{u}_2 = (u_3)_Z$ and $\dot{u}_3 = U_{tt}$ obtained from (23). Denote $\mathbf{u} = (u_1, u_2, u_3)$.

It might be tempting to write the system in terms of a conservative flux and a source term, $\mathbf{u}_t = f(Z, t, \mathbf{u})_Z + s(Z, t, \mathbf{u})$, where $f(Z, t, \mathbf{u})$ is the flux of the conservative hyperbolic system, and the term $s(Z, t, \mathbf{u})$ is the source (e.g., [13]), but the flux cannot easily be found in closed form.

To estimate the required magnitude of the time step to obtain the response during the plunger displacement, temporarily assume that the volume fractions of the phases remain constant and assume a linearly elastic solid phase so that the unsteady hyperbolic biphasic equation has the quasi-linear form, $c(1 + U_Z)^{-1} U_{ZZ} + a U_{tt} + b U_t = d$. Note that in this approximation, the biphasic quasi-linear equation is of the form of the wave equation with velocity $\sqrt{-c(1 + U_Z)^{-1}/a}$. This velocity expression is also the eigenvalue of the matrix A when this approximation to the unsteady biphasic partial differential equation is written in the Lax form $\dot{\mathbf{u}} = A U_Z + S$ [17]. Here, for the constant rate plunger displacement regime, choose $dt = 0.001(0.9)dZ/max$ to be the constant time step size with a Courant–Friedrichs–Lewy (CFL) number of 0.9, where $max = \sqrt{-c(1 + 0.5)^{-1}/a}$ since the average magnitude of $|U_Z|$ is chosen as 0.5. Note that $a < 0$.

Hyperbolic systems can be solved rapidly by explicit finite difference schemes. Numerical dissipation [30, Def. 5.1.1] in finite difference schemes for hyperbolic partial differential equations decreases the amplitude of frequencies of the solution inaccuracies at one time that cause errors in the solution in the next time step. In particular, numerical dissipation reduces high frequency noise in the computed solution. The original Lax–Friedrichs (LxF) scheme is not dissipative, but Shampine [25] has developed a two-step variation of the Lax–Friedrichs scheme that is second-order dissipative. The solution on the original mesh arises from a half step taken with LxF on a staggered mesh and a second half step taken with LxF.

Here, the hyperbolic governing equation (23) is solved by the Shampine finite difference scheme, available in Matlab code for systems of first-order hyperbolic pdes, provided by Shampine [24] for this variant of the Lax–Friedrichs (LxF) scheme. This package also includes versions of the Lax–Wendroff and the Nessyahu–Tadmor methods, but they do not produce physically reasonable solutions of (23).

Because only the Lie time derivative of a velocity, and no strain tensor, is involved in the derivation of the hyperbolic partial differential equation (23), the problem of lack of work-conjugacy that causes errors in some finite element method computations [14] does not arise in this finite differences calculation.

5 Response of the unsteady biphasic model

The unsteady biphasic governing hyperbolic equation (23) predicts the local solid phase displacements during a standard confined compression test. The following parametric study investigates the response under a six decade range of constant global strain rates, 0.001/s, 1/s and 1,000/s, induced by constant rate displacement of the plunger at $\dot{\epsilon}h$ to produce a strain rate $\dot{\epsilon}$ in a specimen that has length h . The parametric study is primarily focused, at these plunger displacement rates, on the effect of the unsteady parameter τ , for various constant

permeability values, and for linear elastic or viscoelastic solid phase stress–stretch relations, on the solid phase displacement distribution. The response to the constant rate displacement of the plunger is considered separately from stress relaxation and in each case is compared with the equilibrium state.

If the specimen were in equilibrium at the end of the plunger displacement, the magnitude of the local solid phase displacement, $U(Z, t)$, at that stage would decrease linearly in Z from the displacement at the plunger to zero at the base. In equilibrium, the local stretch is constant, $\lambda(Z) = 1 - (d/h)$, throughout the specimen, where h is the original specimen dimension in the direction of the plunger displacement and where $d > 0$ is the plunger displacement. The moderate and high plunger displacement rates and the unsteady fluid behavior produce deviations from this equilibrium configuration at the end of a constant rate plunger displacement regime and then, if the plunger is held in position, this displacement field relaxes to equilibrium in a fairly short time due to fluid redistribution.

In the numerical studies presented below, the specimen length is $h = 3$ mm and the final plunger displacement is 0.0006 mm to create a finite deformation with a global compressive strain of 20%. The initial fluid volume fraction is $\Phi_o^f = 0.8$ and the masses of the fluid and solid phases are taken to be 1,000 and 1,040 kg/m³, respectively, similar to brain tissue.

For the case of a linearly elastic solid phase, the compressive linear elastic modulus is chosen to represent one of three hydrated materials: brain tissue, 10 kPa [29]; 4% agarose gel, 10 kPa, [6]; and cartilage, 0.55 MPa, [28]. Constant permeability values from the literature are assumed: brain, 10^{-10} to 10^{-14} , [3, 5, 15]; 4% agarose gel, 6.6×10^{-14} , [6]; cartilage, 5×10^{-16} , [16].

5.1 The specimen non-equilibrium state and the pressure distribution

The plunger displacement forces the interstitial fluid from its initial state and produces large non-uniform fluid hydrostatic pressures, which induce the bulk viscoelastic response by causing a fluid–solid interaction and drive stress relaxation from fluid redistribution. Because the specimen is in a non-equilibrium state during its deformation, particularly at moderate and high plunger displacement rates, and also during relaxation, the total stress, σ_t , at each point of the specimen may not be equal to the experimentally measured stress at the load cell attached to the plunger (Fig. 1). The total stress is uniform over the specimen only when the system is in equilibrium, or when the acceleration terms are neglected, say by ignoring the mass as done by Holmes [10]. However, at each point, the total stress is the sum of the stress in the solid phase, σ^s , and the hydrostatic pressure, p , in the fluid by the mixture theory assumption, $\sigma_t = \sigma^s + p$.

During the plunger displacement, the hydrostatic fluid pressure differential across the plunger interface must be nonzero to ensure fluid flow from the specimen. Likewise, the interface pressure differential may or may not be zero during bulk stress relaxation or creep because the bulk tissue is not in equilibrium, and fluid may still exit the bulk tissue. When the bulk tissue has relaxed to equilibrium, the hydrostatic pressure still may not be zero if some pressure is needed to balance residual stresses in the bulk tissue. In contrast, Mow et al. [21] argue that, in creep with a free draining plunger, the pressure at the interface is zero because the plunger is stationary, and therefore, the solid phase carries all the stress. To compute the pressure at the base during a confined compression test, in addition to taking the local pressure zero at the free draining plunger, Soltz and Ateshian [28] also assume that the total stress, σ_t , is constant throughout the specimen; these assumptions are at best an approximation even though the bulk tissue could have been close to equilibrium throughout the test because their plunger displacement was quite slow. However, the non-equilibrium state has traditionally not been explicitly discussed.

In principle, the total stress distribution at each time is obtained from conservation of linear momentum for the bulk tissue (9) which relates the total stress at each point, but requires knowing the acceleration of each point of the solid phase from the hyperbolic governing equation and then the acceleration of the fluid from the continuity equation, $\phi^s v^s + \phi^f v^f = v_o$. The solution of (9) for the total stress at each Z may require experimental measurement of the solid phase stress at the plunger to produce a boundary condition. If such a solution could be achieved, which is not done in this paper, the local pressure field $p(Z)$ is also computable from $\sigma_t = \sigma^s + p$ because the stress in the solid phase at each point is $\sigma^s(\lambda)$, where $\lambda = 1 + dU/dZ$ is known from the computed displacement field.

5.2 Solid phase response to constant rate plunger displacement

To investigate whether the unsteady biphasic hyperbolic equation (23) predicts physically reasonable displacements at moderate to high rates of the plunger displacement, first assume that the solid phase is linearly elastic.

Table 1 Solid phase local stretch after a constant rate plunger displacement

Rate (/s)	E (kPa)	K (m^4/Ns)	τ (s)	λ_p	λ_m	λ_b
0.001	10	10^{-12}	0.0001	0.799	0.801	0.798
0.001	10	10^{-12}	0.001	0.7996	0.8019	0.7944
0.001	10	10^{-12}	0.01	0.797	0.806	0.783
0.001	10	10^{-14}	0.01	0.774	0.855	0.637
0.001	10	10^{-12}	0.05	0.797	0.813	0.761
0.001	10	10^{-14}	0.05	0.707	0.907	0.484
0.001	10	10^{-12}	0.5	0.786	0.841	0.681
0.001	10	10^{-14}	0.5	0.508	0.984	0.1257
0.001	10	10^{-12}	1	0.774	0.855	0.637
0.001	10	10^{-14}	1,000	0.293	0.829	0.622
0.001	550	10^{-12}	0.0001	0.800	0.801	0.7998
0.001	550	10^{-12}	1	0.798	0.808	0.777
0.001	550	10^{-14}	1	0.757	0.871	0.591
0.001	550	10^{-12}	2	0.798	0.811	0.767
0.001	550	10^{-14}	2	0.735	0.893	0.529
1	10	10^{-8}	0	0.799	0.802	0.794
1	10	10^{-10}	0.000001	0.799	0.806	0.781
1	10	10^{-10}	0.0001	0.774	0.855	0.637
1	10	10^{-10}	0.0005	0.707	0.907	0.484
1	10	10^{-10}	0.001	0.664	0.932	0.405
1	10	10^{-10}	1	0.293	0.829	0.622
1	10	10^{-12}	1	0.293	0.829	0.622
1	10	10^{-14}	1	0.293	0.829	0.622
1	550	10^{-10}	0	0.7999	0.8003	0.7991
1	550	10^{-10}	0.001	0.794	0.825	0.726
1	550	10^{-10}	0.01	0.755	0.871	0.594
1	550	10^{-12}	0.01	0.311	1.0	-0.206
1	550	10^{-12}	0.5	0.181	0.847	0.311
1	550	10^{-15}	0.5	0.181	0.847	0.311
1	550	10^{-10}	1	0.571	0.829	0.730
1	550	10^{-12}	1	0.293	0.829	0.622
1	550	10^{-14}	1	0.293	0.829	0.622
1	550	10^{-16}	1	0.293	0.829	0.622
1	550	10^{-12}	1.5	0.335	0.822	0.739
1,000	10	10^{-10}	0.0005	0.181	0.847	0.311
1,000	10	10^{-14}	0.0005	0.181	0.847	0.311
1,000	550	10^{-10}	0.0005	0.181	0.847	0.311
1,000	550	10^{-14}	0.0005	0.181	0.847	0.311

In Table 1, E is the elastic modulus, K is the constant permeability, and τ is the unsteady coefficient. The predicted stretches are given at three locations in the specimen after the constant rate displacement of the plunger is completed, λ_p is the predicted stretch at the plunger, λ_m is the peak stretch value in the middle region of the specimen (its position varies), and λ_b is the stretch at the base. Because the plunger is displaced through $0.2h$, the equilibrium state is stretch of 0.8 throughout the specimen.

For some combinations of parameters, when τ is too large or the rate is too large, the numerical scheme predicts a physically impossible negative stretch at the base, indicating that the material has been crushed. For other combinations of parameters, the numerical method fails to yield numerical values for the displacement. No computation of the effect of including the masses versus no mass, as in the parabolic equation, is possible because the Shampine finite difference scheme is specialized for hyperbolic equations and so cannot be applied to the parabolic equation case of zero mass and $\tau = 0$.

The general pattern in the solid displacement distribution at the end of the constant rate plunger displacement for all rates is a monotonic, but not linear, decrease with respect to Z from the plunger to the base. Furthermore, the distribution is not symmetric about the mid-plane of the specimen because the plunger is moving against one end while the supporting base at the other end of the specimen is fixed. At the ends of the specimen, the local compressive strain is larger than the equilibrium compressive strain, while in the mid-region of the specimen the compressive strain is less than equilibrium. The relative magnitudes of the local compressive

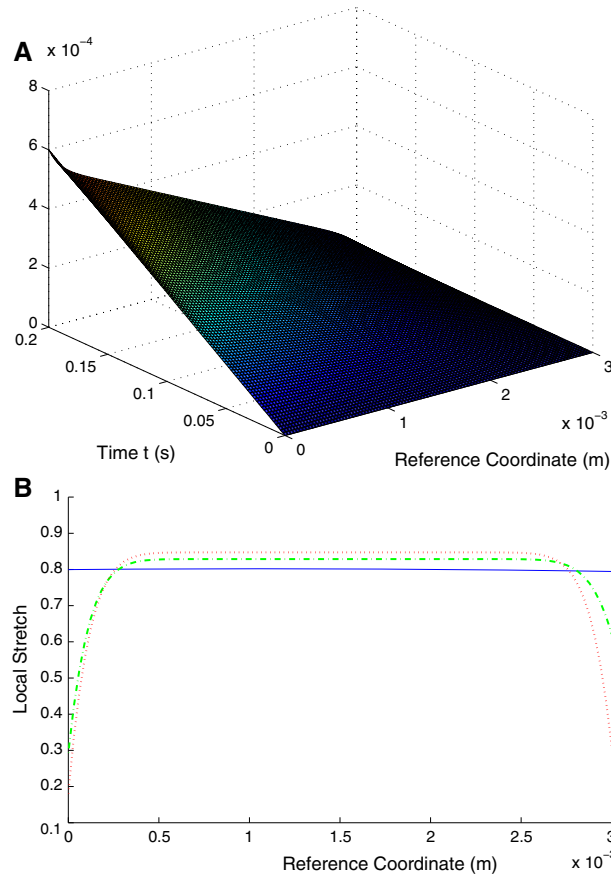


Fig. 3 **a** The displacement distribution of the solid phase with $E = 10$ kPa, $K = 10^{-12}$, and $\tau = 1$ during the displacement of the plunger at 1/s. **b** The predicted rate-influenced solid phase local stretch distribution of the unsteady model versus Z at the end of a constant plunger displacement to 0.2 global strain for a solid phase with $E = 10$ kPa, $K = 10^{-12}$. The *blue solid curve* is for 0.001/s and $\tau = 0.001$. The *green dot-dash curve* is for 1/s and $\tau = 1$. The *red dotted curve* is for 1,000/s and $\tau = 0.0005$ (color figure online)

strains at the ends of the specimen depend on the values of τ and the plunger displacement rate (Table 1). Since increasing τ increases the drag force, at all rates, a larger value of τ produces a greater compressive strain at the ends, a fact which is consistent with the assumed importance of the fluid motion in the mechanical response. At the slow rate 0.001/s for small τ and a linearly elastic solid, the local solid phase displacement field at the end of the plunger displacement is nearly linear and is close to equilibrium. However, a moderate rate of the plunger displacement moves the computed solid phase displacement field away from equilibrium as the plunger displaces (Fig. 3a). In general, the compressive strain at the ends of the specimen tends to increase with increasing plunger displacement rate (Fig. 3b).

Furthermore, under the slow or moderate plunger displacement with small τ , a decrease in stiffness E or permeability K increases the compressive strain at the ends of the specimen. A larger solid permeability decreases the drag force from the relative velocity between solid and fluid phases and therefore reduces these solid phase displacements. However, at 1,000/s, the elastic modulus and permeability in the ranges chosen make no significant difference in the displacement distribution at the end of the ramp load (Table 1). The numerical solution to the hyperbolic governing equation (23) does not predict shock waves during the plunger displacement stage at the high 1,000/s strain rate. However, the smoothing induced by the dissipative numerical scheme might obscure any that exist physically.

5.2.1 Solid phase stress evolution at the plunger

While the hydrostatic pressure contribution to the non-equilibrium total stress at the plunger cannot be computed directly from the non-equilibrium hyperbolic governing equation, the evolution of the stress carried by the

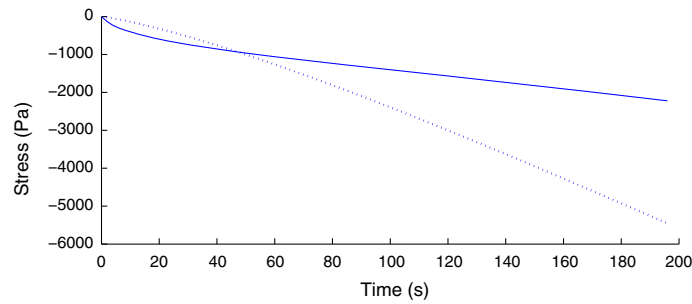


Fig. 4 An increase in τ changes softening to hardening by as reflected in the concavity of the stress in a linear elastic solid phase at the plunger during the constant rate plunger displacement in the case of a constant permeability of 10^{-12} and $E = 10$ kPa. The solid curve is 0.001/s, $\tau = 1$ and the dotted curve is 0.001/s, $\tau = 500$

solid phase is predicted by applying the solid constitutive model to the strain dU/dZ at the plunger for each time step. Here, the strain at a given time is approximated by the difference of the two displacement values closest to the plunger divided by $\Delta Z = h/100$.

The magnitude of τ determines whether the model predicts hardening or softening in the stress response at the plunger. The hyperbolic governing differential equation predicts softening at low and moderate rates for which the parameter, τ , is small, where the flow is nearly steady. However, even at the slow plunger displacement rate of 0.001/s, the predicted response can be made to be hardening by increasing $\tau > 100$ in the case of a constant permeability of 10^{-14} and $E = 10$ kPa. Also, at 1/s with a large elastic modulus of $E = 550$ kPa, constant permeability of 10^{-12} , and $\tau \geq 1.0$ or at high rates of 1,000/s, the hyperbolic governing equation predicts hardening (Fig. 4).

A larger magnitude of τ increases the drag force. Models based on the Darcy relation achieve hardening by making the permeability a nonlinear function to increase the drag force during loading. For example, in the classical studies of cartilage permeability, the strain softening predicted by the parabolic equation for the linear theory was successfully adjusted to represent the experimentally observed hardening in the stress response at the plunger by assuming an exponential relationship, $K = K_o \exp[M\epsilon]$, between permeability, K , and strain, ϵ , physically an assumption that paths for fluid transport are narrowed as the strain increases (e.g., [16,21]). Other models based on the assumption that the fluid obeys the steady flow Darcy relation postulate different functional forms for the permeability (e.g., [6, 11, 19]). The interaction of unsteady flow and nonlinear forms of the permeability that depend on other parameters remains for further study. The drag force may also include a contribution due to breaking and reformation of adhesions in the tissue as suggested by Preziosi and Vitale [23], who produce a plasticity-like model that assumes a threshold value for adhesion rupture.

An experimental hardening response is not universal for hydrated soft tissue because rat brain tissue exhibits softening at slow and moderate rates in the experimental confined compression test (Haslach et al. [9]). The hyperbolic governing equation at slow and moderate rates captures softening behavior for values sometimes assumed for brain tissue, $E = 10$ kPa and $K = 10^{-14}$, and small τ .

5.2.2 Influence of a solid phase viscoelastic stress–stretch relation

To investigate how a viscoelastic solid phase constitutive relation influences the solid displacement response in contrast to larger values of τ , consider a linear viscoelastic solid phase, one whose stress–strain response obeys superposition and one for which the stress is proportional to the strain at a given time, t , in the sense that $\sigma(\alpha\epsilon(t)) = \alpha\sigma(\epsilon(t))$. The standard solid, three-element linear viscoelastic model (28) of a spring (E_1) in series with a Kelvin–Voigt model (E_2, c) was used to represent axonal axial deformation in brain tissue by Dennerll et al. [4],

$$\dot{\sigma} + \frac{(E_1 + E_2)}{c}\sigma = E_1\dot{\epsilon} + \frac{E_1 E_2}{c}\epsilon. \quad (28)$$

The term needed in the biphasic hyperbolic partial differential Eq. (23) is $\partial\sigma_v/\partial\lambda \equiv \sigma_\lambda$ rather than the stress. Assume that σ is a function of both time, t , and stretch, λ , substitute $\epsilon = \lambda - 1$ in (28), and implicitly differentiate the resulting differential equation with respect to λ . A short computation yields the solution for $\sigma_\lambda(t)$,

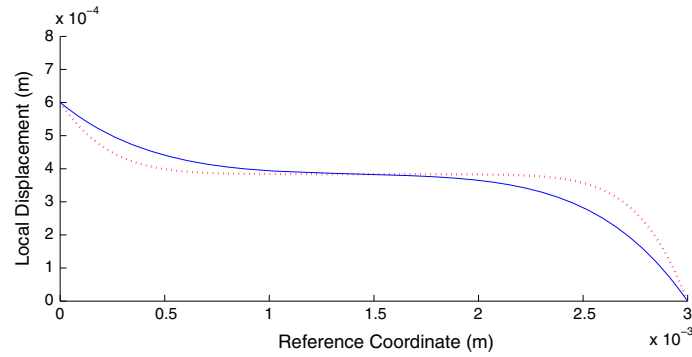


Fig. 5 The solid phase local displacements over a specimen of length 3 mm at the end of the constant 1/s rate plunger displacement for **a** a linearly elastic solid phase with $E = 220$ kPa, $\tau = 0.001$, and $K = 10^{-12}$ (*solid blue*) **b** prediction for the standard solid (30) with $c = 9$ MPa $^{-s}$ with $\tau = 0.001$, and $K = 10^{-12}$ (*dotted red*). The viscoelastic solid phase allows larger compressive strains at the ends of the specimen (color figure online)

$$\begin{aligned}\sigma_\lambda(t) &= \sigma_\lambda(0) \exp[-(E_1 + E_2)t/c] + \frac{E_1 E_2}{E_1 + E_2} [1 - \exp[-(E_1 + E_2)t/c]] \\ &= \frac{E_1^2}{E_1 + E_2} \exp[-(E_1 + E_2)t/c] + \frac{E_1 E_2}{(E_1 + E_2)},\end{aligned}\quad (29)$$

if $\sigma_\lambda(0) = E_1$ as estimated by solving the standard solid model when $\epsilon = rt$, where r is the constant strain rate.

Since the strain in the solid phase is not proportional to time even when the plunger displacement is, a means to compute $\sigma_v(\epsilon)$ is required to estimate the solid phase stress near the plunger. If the stress depends on varying λ , then $\dot{\sigma}(t) = \sigma_\lambda(t)\dot{\epsilon}$ by the chain rule. In this case, the standard linear solid viscoelastic stress in the solid phase is obtained from (28) as

$$\sigma_v(\epsilon) = -\frac{c}{E_1 + E_2} \sigma_\lambda(t)\dot{\epsilon} + \frac{cE_1}{E_1 + E_2} \dot{\epsilon} + \frac{E_1 E_2}{E_1 + E_2} \epsilon. \quad (30)$$

Note that since $\sigma_\lambda(0) = E_1$, $\sigma_v(0) = 0$ at $\epsilon = 0$.

As an example to match the proportions of the Dennerll [4] standard solid model for axonal deformation, let the standard solid parameters, $E_1 = 210$, $E_2 = 10.5$ kPa and $c = 9$ MPa $^{-s}$, be chosen by assuming that $E_1 = 20E_2$ that the equilibrium state has modulus $E_1 E_2 / (E_1 + E_2) = 10$ kPa and that the ratio $(E_1 + E_2)/c = 1/40$. Under these values, the viscoelastic slope decreases from about 210 kPa to about 10 kPa in about 200 s. Decreasing c reduces the relaxation time proportionally.

Because the stress response is proportional to the strain rate for a linear viscoelastic solid phase, for this highly dissipative standard solid, the plunger displacement rate change from 0.001/s to 1/s to 1,000/s, increases the predicted stress magnitude at the plunger, when the plunger displacement reaches $0.2h$, from less than 10^4 Pa under 0.001/s by a factor of 1,000 for the moderate rate and to on the order of 10^{10} Pa in the 1,000/s case when $\tau = 0.001$ and $K = 10^{-10}$. The viscoelasticity of the solid phase induces substantial softening at the moderate rate as the deformation proceeds, but produces much less softening in the 1,000/s case. The compressive strain under a plunger displacement of 1/s or 1,000/s reaches 0.336 and 0.707, respectively, next to the plunger while softening because $\sigma_\lambda(t)$ also decreases with time.

Such a viscoelastic material has little influence on the solid phase displacement predicted during the slow 200 s plunger displacement to $0.2h$ at 0.001/s for $h = 3$ mm; a linear elastic solid with $E = 10$ kPa produces the same final solid phase displacement field if $\tau = 0.001$ and $K = 10^{-12}$ or $K = 10^{-10}$ because the specimen is very close to equilibrium throughout the plunger displacement. But the higher constant 1/s rate plunger displacement to $0.2h$ for $\tau = 0.001$, and $K = 10^{-12}$ predicts solid phase local displacements over a specimen of length $h = 3$ mm at the end of the plunger displacement for a linearly elastic solid phase with $E = 220$ kPa that differ from this standard solid with $c = 9$ MPa $^{-s}$ (Fig. 5).

Table 2 Stress relaxation at the end of the constant rate plunger displacement when the solid phase is linearly elastic

Rate (/s)	E (kPa)	K (m^4/Ns)	τ (s)	Relax time (s)	Initial overshoot
0.001	10	10^{-12}	0.0001	0.1	No
0.001	10	10^{-12}	0.001	1	No
0.001	10	10^{-12}	1	20	No
0.001	10	10^{-14}	1	30	Yes
0.001	550	10^{-12}	0.0001	0.01	No
0.001	550	10^{-12}	1	20	Yes
0.001	550	10^{-14}	1	24	Yes
0.001	550	10^{-12}	2	21	No
0.001	550	10^{-14}	2	40	Yes
1	10	10^{-8}	0	0.02	No
1	10	10^{-9}	0	0	No
1	10	10^{-10}	0.0001	0.85	Yes
1	10	10^{-10}	0.001	3	Yes
1	10	10^{-12}	0.001	20	Yes
1	10	10^{-12}	1	30	Yes
1	550	10^{-10}	0	0	No
1	550	10^{-10}	0.0001	0.09	No
1	550	10^{-10}	0.01	1.13	No
1	550	10^{-12}	0.01	20	Yes
1	550	10^{-10}	1	10	Yes
1	550	10^{-12}	1	30	Yes
1,000	10	10^{-10}	0.0005	Blows up	Yes
1,000	10	10^{-14}	0.0005	Blows up	Yes
1,000	550	10^{-10}	0.0005	Blows up	Yes
1,000	550	10^{-14}	0.0005	Blows up	Yes

5.3 Bulk tissue relaxation

The hydrated bulk tissue specimen stress relaxes, as measured by the load cell at the plunger (Fig. 1), when the plunger displacement stops so that the global strain over the full specimen is fixed. However, the local strains in the tissue vary with time as the solid phase displacements, under constant global strain, approach equilibrium, largely due to fluid redistribution.

To predict the local displacements of the solid phase during stress relaxation of the bulk tissue, the displacement rate of the plunger is set to zero in the hyperbolic governing equation (23). The initial condition for relaxation is the final state of the local displacements during the previous constant rate of plunger displacement computation, which is often far from equilibrium in the hyperbolic equation prediction, in contrast to the prediction of the steady flow equation at slow rates so that the steady and unsteady cases begin relaxation from different initial conditions. The boundary conditions are that the displacement is fixed at the plunger and is zero at the base during relaxation. The time step interval for relaxation is set to be 0.005 s in the Shampine numerical scheme. The amount of time that the system is allowed to relax is an input to the program so that it is a matter of trial and error to estimate the time required to reach global equilibrium. The time-position surface of the solid phase displacement and the time evolution of the stress in the solid phase at the plunger describe the relaxation. The numerically predicted relaxation of the solid phase to the equilibrium constant local stretch that is equal to the global stretch computed from the displacement of the plunger, as is expected physically, validates the numerical method for the hyperbolic equation. The relaxation computations in Table 2 are continuations of some of those in Table 1 with the same geometric properties.

The relaxation time is the time required for the solid phase to nearly reach the equilibrium state corresponding to the plunger displacement, but the bulk tissue should reach equilibrium at the same time. The relaxation times tend to be shorter after a slower constant rate plunger displacement because the relaxation begins from a state closer to equilibrium. The reported relaxation time is 1–4 s in bovine cartilage [20], a value consistent with the predicted relaxation times after 0.001/s plunger displacement and small τ . The relaxation times, estimated from the graph of the relaxation of the solid phase next to the plunger, are longer when τ is greater because the system during both stages is further from the equilibrium state in which no fluid redistributes. The relaxation time is also longer with a smaller permeability and with smaller elastic modulus for the same reason.

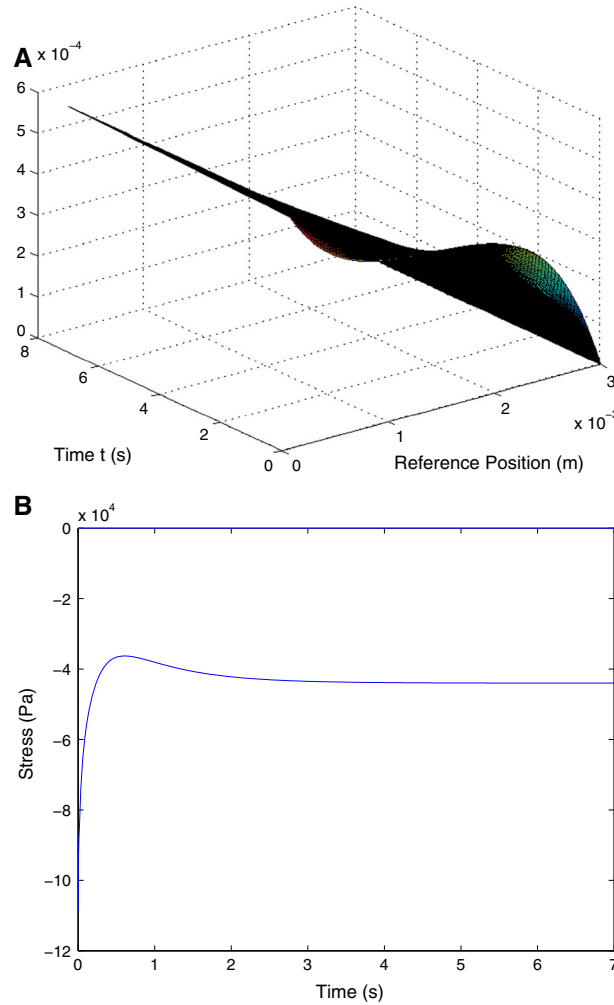


Fig. 6 **a** Initial overshoot of the relaxation stress at the plunger during 7 s for a linearly elastic solid phase with $E = 220$ kPa, $\tau = 0.001$, and $K = 10^{-12}$. The preceding plunger displacement was at 1/s. **b** Overshoot of the solid phase relaxation displacement at the plunger for relaxation for 7 s when the solid phase is linearly elastic with $E = 220$ kPa, $\tau = 0.001$, and $K = 10^{-12}$. The preceding plunger displacement was at 1/s

Under some choices of the parameter τ , the computation predicts that, even after the plunger stops moving, the induced displacements at most points in the solid phase continue to increase for a short period of time, especially in the less compressed mid-region of the specimen, a non-equilibrium response that can best be called overshoot from the plunger displacement. The yes or no in Table 2 characterizes the presence of overshoot at the beginning of relaxation. The overshoot is a mathematical result of the abrupt stop of the plunger motion that has accelerated the solid and fluid, but in an experiment conducted on a testing machine, the machine slows the plunger before stopping it for relaxation so that no overshoot appears in the experimental data. Small values of τ predict modest overshoot, and larger values of τ predict greater overshoot displacements. The unrealistically large predicted overshoot on the order of meters at 1,000/s with small τ may be due to the numerical method or to a limitation of the model, but no experimental guidance is available for confined compression of hydrated soft tissue at 1,000/s.

Another solid phase overshoot may occur at the end of stress relaxation due to the assumed fluid acceleration measured by τ , because the relaxation stress in the solid phase at the plunger often drops suddenly and overshoots equilibrium in a very short period of time. The stress magnitude in the solid phase then increases slowly back to equilibrium. For example, after a plunger displacement of 1/s and with parameters $\tau = 1$ for the fluid acceleration, $K = 10^{-12}$ and $E = 220$ kPa the large initial overshoot (Fig. 6a) is reflected in overshoot of the stress in the solid phase next to the plunger in its relaxation to equilibrium before eventually

approaching the negative equilibrium stress (Fig. 6b). In this example, the solid phase displacement after the end of the plunger displacement is close to equilibrium, but the fluid acceleration initially drives the system away from equilibrium before returning to equilibrium. Such overshoot is rarely detected in experiment. The numerical method fails if τ is set to zero or if τ is forced to decrease to zero during relaxation to remove the fluid acceleration. Either type of predicted overshoot in the relaxation stage may possibly be reduced by use of a nonlinear permeability function that varies the drag force appropriate to the tissue tested, but such functions have not yet been explored for unsteady flow.

5.3.1 Linear viscoelastic solid phase relaxation

The relative contribution of viscoelastic solid phase relaxation during the fluid rearrangement in the stress relaxation of the bulk material is to slow the relaxation to equilibrium compared with a linearly elastic solid phase, as also determined by Mak [18] for the average stress over the whole specimen. For example, at the moderate rate of 1/s, a tissue with standard linear solid phase (28), where $c = 9 \text{ MPa}^{-\text{s}}$ with $\tau = 0.001$, and $K = 10^{-12}$ takes the longer time of about 25 s to -2 kPa equilibrium than the 7 s to -44 kPa equilibrium of a tissue with linearly elastic solid phase with $E = 220 \text{ kPa}$, $\tau = 0.001$, and $K = 10^{-12}$. In the viscoelastic case, the stretch values at the end of the plunger displacement are $\lambda_p = 0.1294$, $\lambda_m = 1.0$, $\lambda_b = -0.545$ so that the lower 0.00012 mm of the specimen is crushed and in the linear elastic case are $\lambda_p = 0.506$, $\lambda_m = 0.983$, $\lambda_b = 0.1226$ where the stretches have the same meaning as in Table 1. Of course if the solid is linearly elastic, all change of solid phase displacements during the bulk tissue stress relaxation is due to fluid redistribution, since a linearly elastic solid phase would relax to equilibrium immediately if not for drag from the fluid phase.

6 Conclusion

This study investigates the effect of assuming unsteady flow, under high plunger deformation rates, on the predicted response for confined compression tests of hydrated soft biological materials. The hyperbolic governing equation proposed produces a more complete non-equilibrium description of the confined compression experiment for hydrated soft biological tissue loaded under moderate to high rates than the slow rate parabolic approximation made by cartilage researchers because the hyperbolic governing equation does not predict instantaneous propagation of disturbances and because it allows unsteady flux of the internal fluid by replacing Darcy steady flow with an unsteady flow model. This study further raises the question of how the possible dependence of the permeability on the stretch or on other parameters is related to the assumption of unsteady flow.

Acknowledgments This work was supported in part by a University of Maryland SEED grant and by the Center for Energetics Concepts Development of the University of Maryland - College Park.

References

1. Ateshian, G.A., Warden, W.H., Kim, J.J., Grelsamer, R.P., Mow, V.C.: Finite deformation biphasic material properties of bovine articular cartilage from confined compression experiments. *J. Biomech.* **30**, 1157–1164 (1997)
2. Carniel, E.L., Fontanella, C.G., Stefanini, C., Natali, A.N.: A procedure for the computational investigation of stress-relaxation phenomena. *Mech. Time-Depend. Mater.* **17**, 25–38 (2013)
3. Cheng, S., Bilston, L.E.: Unconfined compression of white matter. *J. Biomech.* **40**, 117–124 (2007)
4. Dennerll, T.J., Lamoureux, P., Buxbaum, R.E., Heidemann, S.R.: The cytomechanics of axonal elongation and retraction. *J. Cell. Biol.* **109**, 3073–3083 (1989)
5. Franceschini, G., Bigonia, D., Regitnig, P., Holzapfel, G.A.: Brain tissue deforms similarly to filled elastomers and follows consolidation theory. *J. Mech. Phys. Solids* **54**, 2592–2620 (2006)
6. Gu, W.Y., Yao, H., Huang, C.Y., Cheung, H.S.: New insight into deformation dependent hydraulic permeability of gels and cartilage, and dynamic behavior of agarose gels in confined compression. *J. Biomech.* **36**, 593–598 (2003)
7. Haslach, H.W. Jr.: Thermodynamically consistent, maximum dissipation, time-dependent models for non-equilibrium behavior. *Int. J. Solids Struct.* **46**, 3964–3976 (2009). doi:[10.1016/j.ijsolstr.2009.07.017](https://doi.org/10.1016/j.ijsolstr.2009.07.017)
8. Haslach, H.W. Jr.: *Maximum Dissipation Non-Equilibrium Thermodynamics and its Geometric Structure*. Springer, New York (2011)
9. Haslach, H.W. Jr., Leahy, L.N., Riley, P., Gullapalli, R., Xu, S., Hsieh, A.H.: Solid—extracellular fluid interaction and damage in the mechanical response of rat brain tissue under confined compression. *J. Mech. Behav. Biomed. Mater.* **29**, 138–150 (2014). doi:[10.1016/j.jmbbm.2013.08.027](https://doi.org/10.1016/j.jmbbm.2013.08.027)

10. Holmes, M.H.: Finite deformation of soft tissue: analysis of a mixture model in uniaxial compression. *J. Biomech. Eng.* **108**, 372–381 (1986)
11. Holmes, M.H., Mow, V.C.: The nonlinear characteristics of soft gels and hydrated connective tissues in ultrafiltration. *J. Biomech.* **23**, 1145–1156 (1990)
12. Holzapfel, G.A.: *Nonlinear Solid Mechanics*, Wiley, Chichester (2000, reprint 2005)
13. Hudson, J: Numerical techniques for conservation laws with source terms, MSc Thesis, University of Reading, UK (1998)
14. Ji, W., Waas, A.M., Bažant, Z.P.: Errors caused by non-work-conjugate stress and strain measures and necessary corrections in finite element programs. *J. Appl. Mech.-T ASME* **77** (July), 044504-1–044504-5 (2010)
15. Kaczmarek, M., Subramaniam, R.P., Neff, S.R.: The hydromechanics of hydrocephalus: steady-state solutions for cylindrical geometry. *Bull. Math. Biol.* **59**, 295–323 (1997)
16. Lai, W.M., Mow, V.C.: Drag-induced compression of articular cartilage during permeation experiment. *Biorheology* **17**, 111–123 (1980)
17. Lax, P.D.: *Hyperbolic Partial Differential Equations*. American Mathematical Society, Providence, RI (2006)
18. Mak, A.F.: The creep of articular cartilage under confined compression: the contribution from the matrix viscoelasticity and the interstitial fluid flow. In: Spiker, R.L. (ed.) *Advances in Bioengineering*, ASME, pp. 39–40 (1984)
19. Meroi, E.A., Schrefler, B.A., Dorigo, M.T.: A computational formulation for coupled response of trabecular meshwork in human eye. In: Papadarakakis, M., Onate, E., Schrefler, B. (eds.) *Computational Methods for Coupled Problems in Science and Engineering*, p47, CIMNE, Barcelona, p. 11 (2005)
20. Mow, V.C.: Biphasic rheological properties of cartilage. *Bull. Hosp. Jt. Dis.* **38**, 121–124 (1977)
21. Mow, V.C., Kuei, S.C., Lai, W.M., Armstrong, C.G.: Biphasic creep and stress relaxation of articular cartilage in compression: theory and experiments. *J. Biomech. Eng.* **102**, 73–84 (1980)
22. Natali, A.N., Carniel, E.L., Pavan, P.G.: A visco-hyperelastic-damage constitutive model for the analysis of the biomechanical response of the periodontal ligament. *J. Biomech. Eng.* **130**, 031004-1 (2008)
23. Preziosi, L., Vitale, G.: A multiphase model of tumor and tissue growth including cell adhesion and plastic re-organization. *Math. Models Methods Appl. Sci.* **21**(9), 1901–1932 (2011)
24. Shampine, L.F.: Solving Hyperbolic PDEs in Matlab. <http://faculty.smu.edu/shampine/hpde> (2005a)
25. Shampine, L.F.: Two-step Lax–Friedrichs method. *Appl. Math. Lett.* **18**, 1134–1136 (2005b)
26. Simo, J.C., Hughes, T.J.R.: *Computational Inelasticity*. Springer, New York (1998)
27. Simon, B.R.: Multiphase poroelastic finite element models for soft tissue structures. *Appl. Mech. Rev.* **45**, 191–218 (1992)
28. Soltz, M.A., Ateshian G.A.: Experimental verification and theoretical prediction of cartilage interstitial fluid pressurization at an impermeable contact interface in confined compression. *J. Biomech.* **31**, 927–934 (1998), Corrigendum 39, 594 (2006)
29. Soza, G., Grosso, R., Nimsy, C., Hastreiter, P., Fahlbusch, R., Greiner, G.: Determination of the elasticity parameters of brain tissue with combined simulation and registration. *Int. J. Med. Robot.* **1**, 87–95 (2005)
30. Strikwerda, J.C.: *Finite Difference Schemes and Partial Differential Equations*, 2nd edition. Society for Industrial and Applied Mathematics (2004)